ACADEMIA ROMÂNĂ
Revue Roumaine de Chimie
http://web.icf.ro/rrch/

Rev. Roum. Chim.,
2017, *62*(8-9), 687-698

Dedicated to the memory of
Professor Victor-Emanuel Sahini (1927–2017)

NANOSIZED $NiFe_2O_4$/KAOLINITE COMPOSITE AS ADSORBENT FOR ORGANIC DYES

Ştefana COJOCARU,[a] Adrian BORHAN,[b] Vasyl MYKHAILOVYCH,[c] Simona CUCU-MAN,[b] Nicoleta MELNICIUC-PUICA,[d] Ovidiu Florin CĂLȚUN,[e] Vasile HULEA,[f] Maria CAZACU,[g] Mircea Nicolae PALAMARU[b] and Alexandra Raluca IORDAN[b]

[a] Faculty of Geography and Geology, Alexandru Ioan Cuza University of Iaşi, 11, Carol I Blvd., 700506, Iaşi, Roumania
[b] Faculty of Chemistry, Alexandru Ioan Cuza University of Iaşi, 11, Carol I Blvd., 700506, Iaşi, Roumania
[c] Institute of Biology, Chemistry and Bioresources, Yuriy Fedkovych Chernivtsi National University, 2, Kotsubinsky Str., 58012, Chernivtsi, Ukraine
[d] Faculty of Orthodox Theology, Alexandru Ioan Cuza University of Iaşi, 9 Closca, 700065, Iaşi, Roumania
[e] Faculty of Phisics, Alexandru Ioan Cuza University of Iaşi, 11, Carol I Blvd., 700506, Iaşi, Roumania
[f] Institut Charles Gerhardt Montpellier, UMR 5253, CNRS-UM2-ENSCM-UM1, Matériaux Avancés pour la Catalyse et la Santé, 8 rue de l'Ecole Normale, 34296 Montpellier Cedex 5, France
[g] "Petru Poni" Institute of Macromolecular Chemistry, 41A, Gr. Ghica Voda Alley 700487 Iasi, Roumania

Received December 20, 2016

A magnetic inorganic/inorganic composite material was synthesized by sol-gel autocombustion method, using tartaric acid as fuel. The novelty aspects of the research are represented, firstly, by the combination of nickel ferrite and kaolin clay, and secondly by the employment of sol-gel autocombustion technique to obtain the composite.
The main objective of this work is to characterize the created material and verify its adsorptive/catalytic properties in the decomposition of an organic dye. The structure of the material, which was thermally treated at 350ºC and 500ºC, as well as the formation of spinel structure and the presence of organic species were investigated using infrared absorption spectroscopy (IR). X-ray diffraction (XRD) and scanning electron microscopy (SEM) were used for structural and morphological characterization of samples. The textural properties of the material were examined by nitrogen adsorption–desorption technique, the morphology was studied using transmission electron micrographs (TEM) and the magnetic characteristics were investigated using a vibrating sample magnetometer (VSM). Experiments on the discoloration of methyl orange dye in the presence of the composite materials, determined by UV-Vis spectroscopy, showed very good adsorptive/catalytic properties of material, removing up to 95.8% dye from the solution.

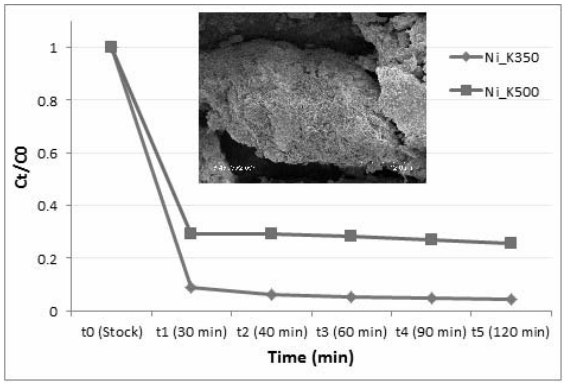

INTRODUCTION

Elimination of organic pollutants from water bodies is an increasingly difficult process, taking into account the enormous quantities of polluting substances eliminated steadily in nature. Methods for treating wastewaters have changed and improved over time, moving from homogeneous to

* Corresponding author: alexandra.iordan@uaic.ro

heterogeneous techniques, *i.e.* photocatalytic degradation, adsorption, extraction, ultra-filtration, ozonation, H_2O_2 oxidation, photo-oxidation, and their combination.[1-5] Adsorption has been found to be an efficient low-cost technique, but it has the disadvantage that the materials used are extremely difficult to remove from water after decontamination.[6] The natural clays and their various modifications are an important class of materials to be used in the removal of organic substances, showing an internal lamellar structure, high specific surface area and a large adsorption capacity of organic and inorganic molecules.[7-8] Generally, in water they swell significantly due to the hydration of the inter-lamellae cations which act as counterions to balance the negative charges of the clay layers. Therefore, inorganic cations in solutions can be intercalated into the interlayer gallery by cation exchange and with the temperature rise occurs the dehydroxylation of hydrated polyoxocations, finally leading to oxide pillars that the clay layer apart.[9] There are three basic classes of clays: kaolinite, micas, and smectites.[2] Although these clays have been extensively studied together with various nanomaterials, to our knowledge there is no report about preparation of kaolinite/$NiFe_2O_4$ nanocomposite. Therefore, this is first report about the adsorptive properties of kaolinite/$NiFe_2O_4$ nanocomposite.

Among various additives, magnetic nanoparticles can be introduced into the clays matrix in order to improve the physical and chemical properties of clay materials[10], *i.e.* adsorption capacity *via* electrostatic interactions and their recovery from effluent. The use of magnetic clays in water treatment is effective, economical and does not lead to the formation of harmful byproducts. One disadvantage is their removal from the environment after adsorption, and the solution to this problem is the introduction of magnetic components in the structure. The separation of the magnetic clay catalysts from the water will therefore be possible by simply applying an external magnetic field. On the other side, the agglomeration tendency of magnetic nanoparticles leads to the increase of their particle size and decrease of their activities as adsorbent or catalyst. Ferrites are a promising class of materials to form clay nano-composites due to their good magnetic properties and nanometric size of particles. Also, ferrites are highly effective catalysts, and the new composite resulted from the combination of the two compounds shows promising features of good adsorbent and catalyst, respectively. Among magnetic nanomaterials, nickel ferrite ($NiFe_2O_4$) with a spinel structure is particularly important because of its potential applications as magnetic material in low regime temperature[11] and catalysts[5]. The structure of 2–3 spinel type oxide with general formula AB_2O_4 is responsible for a variety of interesting properties. Therefore, $NiFe_2O_4$ presents a huge potential for its application in the synthesis of magnetic nanocomposite adsorbents, for dealing with environmental problems. On the other hand, the development of an innovative procedure to prepare a highly homogeneous magnetic metal oxide/clay nanocomposite, to avoid possible release of ferrite from clay matrix into the environment, represents a serious problem. Different techniques have been reported to prepare metal oxide/clay nanocomposites such as molecular self-assembly, co-precipitation[12], sol gel processing[13] *etc*. The sol-gel auto-combustion method appears attractive because of lowering the process temperature, high homogeneity, purity of resulting materials, and possibility of various forming process.[14]

The purpose of this work was to investigate the capability of $NiFe_2O_4$/kaolinite nanocomposites to be used as sorbents for the removal of methyl orange dye from aqueous solution. We have successfully prepared a highly homogeneous phased magnetic $NiFe_2O_4$/kaolinite nanocomposite.

The synthesis via sol-gel autocombustion technique, and the characterization of the novel $NiFe_2O_4$/kaolinite nanocomposite obtained at 350ºC and 500ºC were correlated with relationship between the structural features, the magnetic behavior and the adsorptive capacity.

EXPERIMENTAL

1. Synthesis and characterization of $NiFe_2O_4$/kaolinite nanocomposite

Nanocomposites consisting of $NiFe_2O_4$/kaolinite were prepared in air by sol-gel auto-combustion method using tartaric acid ($C_4H_6O_6$) (Merck) as chelating agent-fuel. Analytical grade precursors, iron nitrate $Fe(NO_3)_3 \cdot 9H_2O$ (Merck), and nickel nitrate $Ni(NO_3)_2 \cdot 6H_2O$ (Merck) were mixed in stoichiometric proportions. A solution of tartaric acid was mixed with metal nitrates mixture in 3:1 molar ratio of tartaric acid to metallic cations. Kaolin clay was purchased commercially and is naturally occurring, originating in a deposit in the Piatra Craiului mountains, Romania. A quantity of kaolinite was mixed with the metal nitrates solution in 3:1 weight ratio of clay to ferrite. The reaction mixture was heated at 75ºC under continuous stirring at 330 rpm in a water bath until gel phase transformation was reached. The dried gel was gradually heated up to 350ºC on the sand bath, where the autocombustion was clearly observed and the gel was converted to powder. The obtained powder was thermally treated up to 500ºC/ 5h (Fig. 1).

Sample	Label
$NiFe_2O_4$/kaolin composite heat treated up to 350°C	Ni_K350
$NiFe_2O_4$/kaolin composite heat treated up to 500°C	Ni_K500

Fig. 1 – $NiFe_2O_4$/kaolinite composite heat treated up to 500°C.

Infrared spectroscopy is a method used to analyze the structure of clays, monitoring the location and intensity of the stretching and deformation bands characteristic to the OH, Si-O and Al-OH bonds. IR spectroscopy was also used for monitoring solid phase chemical reactions and the disappearance of the organic and nitrate phase. FTIR analysis was performed using a Bruker TENSOR TM[27] with ATR cell, with 2 cm^{-1} resolution in infrared range 4000-370 cm^{-1}. XDR and SEM are employed in order to verify the structure formation of nanomaterials. The phase identification of nano powders was done by XRD recorded on Shimadzu LabX 6000 diffractometer equipped with graphite monochromator and Cu$K\alpha$ (λ=1.5406Å) radiation, in the ambient atmosphere with a scanning rate of 0.02º/s over the 2θ = 20–80º range. The morphology of the powders prepared at 350°C was investigated by scanning electron microscopy (SEM) using a Hitachi S2600N Microscope. Textural properties were measured by nitrogen adsorption–desorption isotherms method at 77 K on a Quantachrome Nova 2200 analyzer. Samples were degassed at 250°C for 4 h prior to each measurement. The specific surface area S_{BET} was determined by using the BET method. Magnetic properties of obtained nano powders were investigated at room temperature by using a vibrating sample magnetometer. Transmission electron micrographs (TEM) were obtained on a TESLA 513 A electron microscope. A previous study[15] stands as reference for the characterization of pure kaolinite, as well as kaolinite treated at 350°C and 500°C. The research mentioned showed that the utilized samples of clay are of kaolin-type and contain a large quartz impurity (visible in XRD patterns and FTIR spectra). In the paper it was also stated that applying a temperature higher than 500°C leads to the transformation of kaolin to metakaolin, a phase transition between crystalline and amorphous.

2. Adsorption procedure

The adsorptive capacity of the powders prepared was investigated through the degradation of methyl orange (MO) dye in aqueous solution at constant temperature, under natural visible light. In each reaction, 10 mg of catalyst were added in 25 mL solution of methyl orange ($C_{14}H_{14}N_3NaO_3S$) with an initial concentration of 10 mg/L and pH = 3. The suspension was stirred magnetically at a constant temperature of 23°C. Samples were taken from the suspension at regular intervals (0, 30, 40, 60, 90 and 120 minutes) to investigate the change in the concentration (absorbance) of each degraded solution by measuring the absorbance in range of 250–700 nm for methyl orange dye. Distilled water was used as the reference sample. The absorbance of MO solutions was determined at ~500 nm and it is used to monitor the degradation of dye.

RESULTS AND DISCUSSION

1. Composite Characterization

Infrared Spectroscopy

The IR spectra, in the 4000-370 cm^{-1} wavenumber range of nanocomposites thermally treated at 350°C and 500°C, respectively, are shown in Fig. 2, where the presence of absorption bands characteristic to both clay and ferrite are visible. The absorption bands located below 650 cm^{-1} are attributed to the vibration of metal-oxygen bonds in the structure of nickel ferrite. The maximums observed in the range of 600-470 cm^{-1} are assigned to υ_1 wavenumber (corresponding to metal - oxygen bonds in tetrahedral sites) and those bellow 470 cm^{-1} are attributed to υ_2 wavenumber (corresponding to metal - oxygen vibrations in octahedral positions).[16-17] A shift of the wavenumber value and an increase of bands intensity for both tetrahedral and octahedral vibrations for the sample heated at 500°C is observed. It can be attributed to the complete formation of spinel structure. However, the band located at 1639-1630 cm^{-1} is assigned to the vibration of carboxyl group[18] which means additional thermal treatment is needed to stabilize the structure, but these functional groups are very important to obtain ferrite-clay nanocomposite.

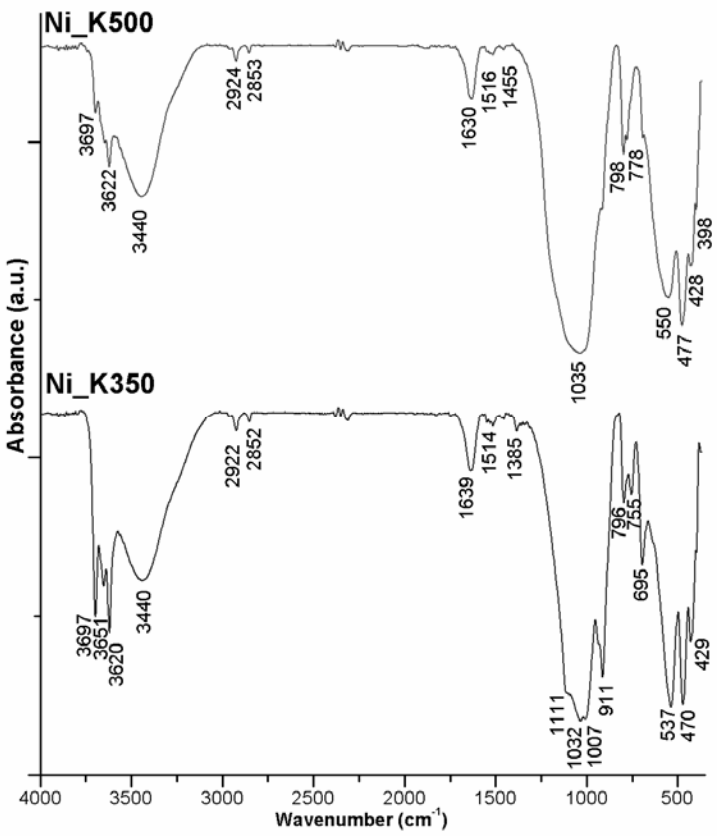

Fig. 2 – IR spectra of the samples.

For kaolinite, the layers of clay are built of a sheet of aluminum octahedrically bonded to oxygen atoms and hydroxyl groups and a sheet of silicon, tetrahedrically bonded to oxygen atoms (siloxane surface).[19] Therefore, bands from 3697, 3651, 3622, 3620, and 3440 cm^{-1} correspond to stretching vibrations of the inner octahedral structure of Al-OH bond. Bands from lower wavenumbers correspond to following bonds: Si-O (1111, ~796, and ~470 cm^{-1}), Si-O-Al (798, 695 and 558cm^{-1}), Al-OH (911 cm^{-1}), and Si-O-Si (~1032 cm^{-1}).[20-21]

The FTIR spectra of samples Ni_K350 and Ni_K500 differ in wavenumbers of Si-O-Si bond which are shifted to higher values (1032 cm^{-1} for Ni_K350 and 1035 cm^{-1} for Ni_K500) according to introduction of $NiFe_2O_4$ in clay sample, which could be related to the change of the bonding characteristics, such as a bond angle.[22] Both samples show typical metakaolinite spectrum, which is characteristic by diminishing of bands at higher wavenumbers belonging to O-H bonds.[23-25]

X-ray Diffraction

The XRD patterns of $NiFe_2O_4$-clay composite (Ni_K350 and Ni_K500) are show in Figure 3. In the case of clay, it is well recognized that well-defined reflections at 2θ value of 12° and 26° corresponding to the (0 0 l) and (0 0 4) Bragg reflections are typical for kaolinite according to the JPCDS 75-1593. The peaks corresponding to the 2θ value intervals 34–40°, 46–50° and 63–70° may vary for kaolinites of different origins.[26]

Other species identified in the structure of clay are quartz and muscovite, the first one being represented by 2θ at 20°, 26° and 60°.The peaks intensity of the kaolinite was found to decrease progressively with the thermal treatment, which is a result of a transformation of crystalline structure in amorphous clay.[27-28] According to Shvarzman *et al.*[29] and Fernandez *et al.*[30], those changes are expected because, with the rise of temperature, dehydroxylation process occurs and subsequent a kaolinite → metakaolinite phase transformation takes place.[31] This new structural form of material usually develops when clay is calcinated over 500-550°C.[32-33] It can be observed that characteristic peaks for quartz (2θ = 21, 27° and 60°) remain unchanged with thermal treatment.[34] The narrowing of the peaks with the thermal treatment may be related to the increase of crystallite size and/or the decrease of the mean lattice strain.[26]

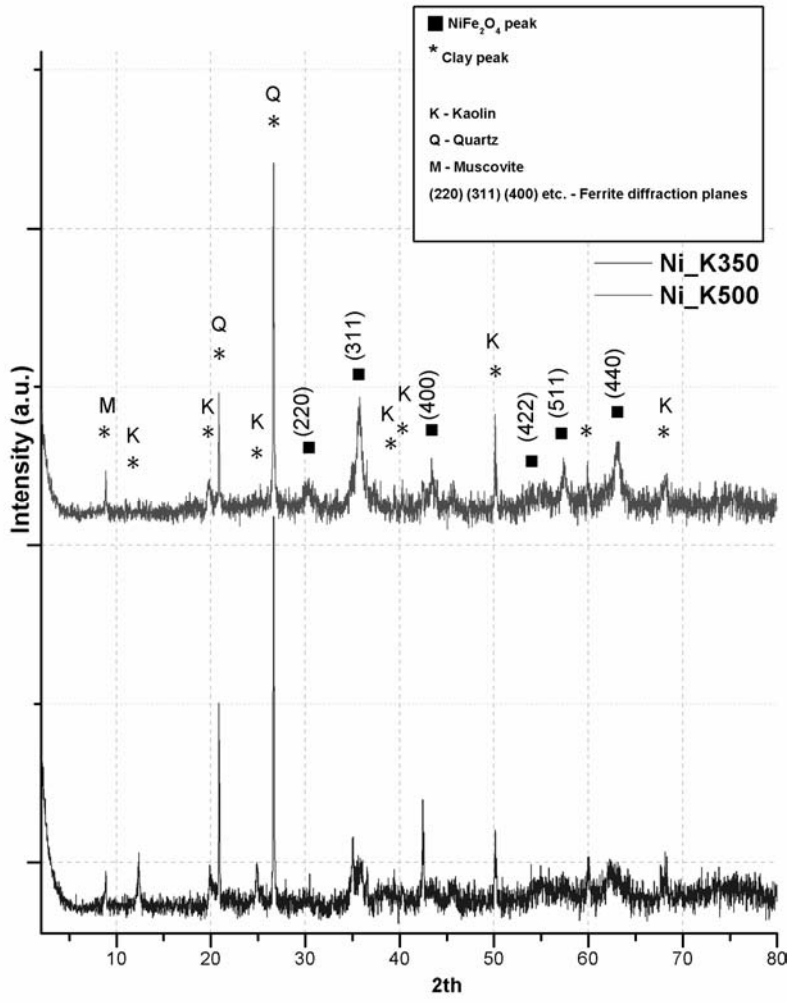

Fig. 3 – XRD pattern of composites.

Table 1

The crystallite size (Dc), lattice parameter (a) and density (ρx) for Ni_K350 and Ni_K500

Sample	Dc (nm)	a (Å)	ρx (g/cm³)
Ni_K350	1927	8.31	5.40
Ni_K500	38.9	8.32	5.38

For the sample treated at 350°C, the structure of nickel ferrite has just begun to form and the characteristic peak located at ~36 2θ is slightly visible. The pattern of the sample obtained at 500°C confirms the formation of single-phase cubic spinel structure. All the reflection peaks were identified and indexed in good agreement with JCPDS 89-4927 and 89-4926.

XRD patterns of the $NiFe_2O_4$-clay composite obtained 500°C show the characteristic peaks appeared at 2θ=26º (corresponding to clay) and 2θ=36º (corresponding to ferrite), and confirm the presence of $NiFe_2O_4$ phase in nanocomposites. The XRD peaks of nickel ferrite nanoparticles are easily observed in XRD pattern of the resulting sample, confirming the successful encapsulation of nickel ferrite nanoparticles within organoclay sheets.

Scanning Electron Microscopy (SEM)

The SEM image of the prepared magnetic Ni_K350 sample (Fig. 4) shows the two components of prepared composite with complete different textures: the flat surface of the clay and the nickel ferrite aggregates. It seems that the $NiFe_2O_4$ nanoparticles are placed on the surface of kaolin. Although an agglomeration of $NiFe_2O_4$ nanoparticles is observed with irregular morphology of aggregates. The holes visible in the image are due to the gas released during auto-combustion process.

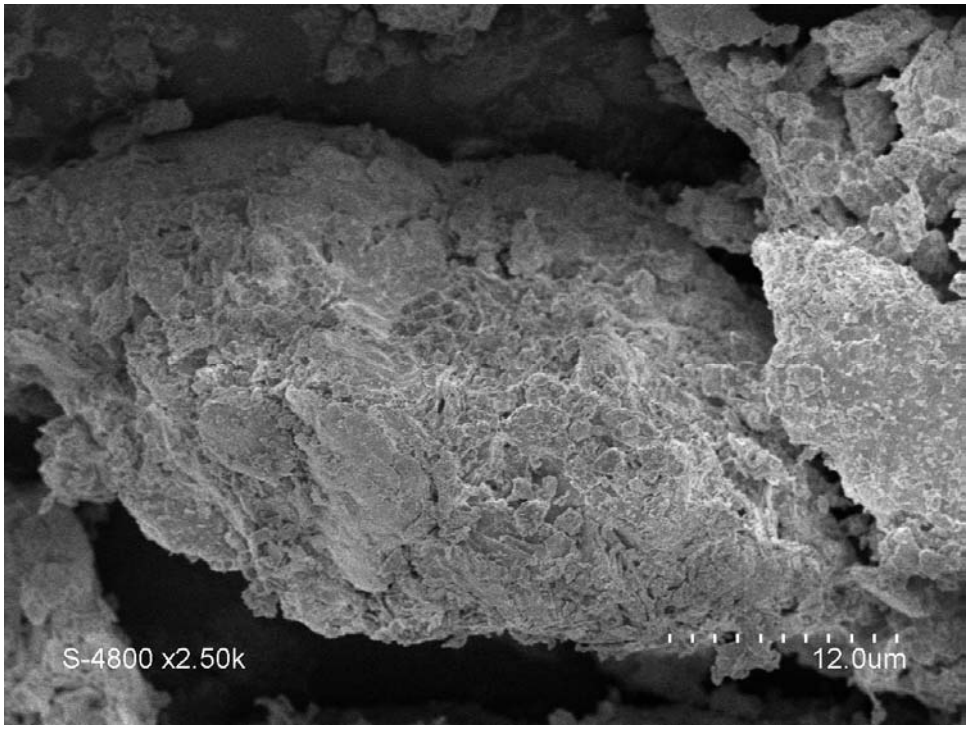

Fig. 4 – SEM image of Ni_K350.

Transmission electron microscopy (TEM)

The morphology of the prepared Ni_K500 composite was studied by TEM technique. The presence of spherical magnetic nanoparticles embedded in the layered structure of clay phase is clearly observed in TEM images (Fig. 5 a and b).

Based on these results, it can be proposed that nickel ferrite particles have been distributed into clusters and located outsides the clay interlayer galleries, which lead to the forming of a mesoporous architecture by stacking of clay layers, as confirmed by N_2 sorption analysis.

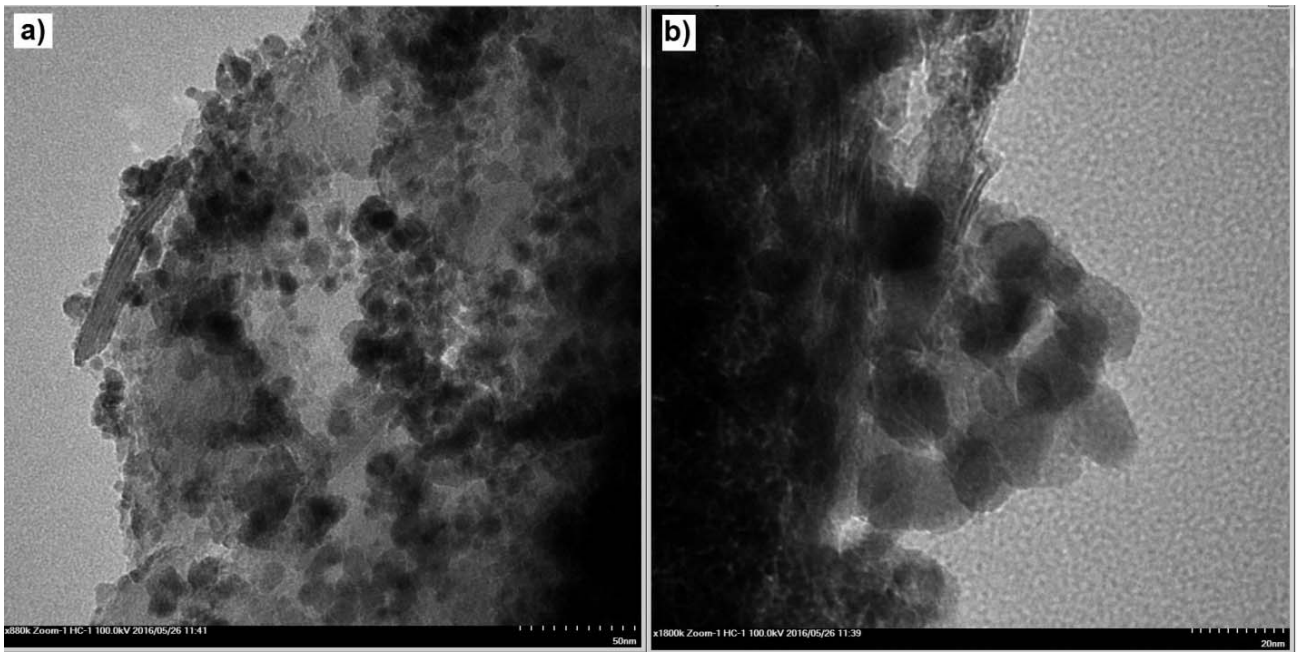

Fig. 5 – TEM image of Ni_K500.

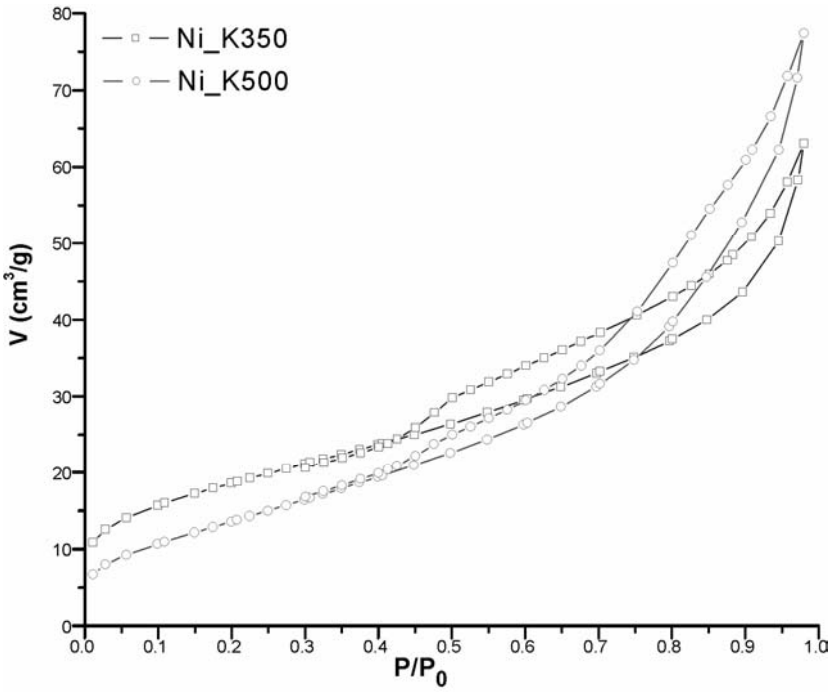

Fig. 6 – Nitrogen adsorption-desorption isotherms for composites.

Table 2

Data obtained from nitrogen adsorption-desorption experiments

Sample	S_{BET} m²/g	Langmuir surface	Pore volume (Adsorption) cm³/g	Pore volume (Desorption) cm³/g	Adsorption average pore diameter (Å)	Desorption average pore diameter (Å)
Ni_K350	66.68	94.29	0.09	0.08	60.11	61.6
Ni_K500	51.47	74.82	0.11	0.11	77.63	73.27

Nitrogen adsorption-desorption

The nitrogen adsorption-desorption experiments were carried out to determine the surface area of the prepared magnetic composite. Nitrogen adsorption–desorption isotherms (Fig.5 (a-b)) of two representative adsorbents (Ni_K350 and Ni_K500) are depicted in Fig. 6. The obtained isotherms can be categorized as type IV with an H3 hysteresis loop according to the IUPAC classifications.[35] This type of isotherms is distinctive of mesoporous materials. A H3-type hysteresis is associated to pores with non-uniform size formed from aggregated or agglomerated particles.[36] The gas uptake sharply increased during the final half of the isotherm, indicating that capillary condensation occurred.[37] In other words, pore diameter and the distribution of pore size which was automatically calculated by the surface area analyzer is wide up to 159 Å. These observations of porous morphology are in good agreement with previous reports.[5,38]

Ni_K350 and Ni_K500 nanocomposites showed BET surface areas of 67 m^2/g and 51 m^2/g, respectively. The BET results corroborated with the XRD and TEM studies indicate that the synthesized magnetic composite can be used as an efficient adsorbent for a dye from water. These features are important for the accessibility of reactant molecules to the catalysts.[39]

Magnetization measurements

After the magnetic composites preparation, a test with a 0.3-T magnet showed that the both materials were magnetic. The magnetic properties of the samples were determined at room temperature by using VSM. Magnetization (M) versus magnetic field (H) curves are shown in Fig. 7. The deduced values of specific magnetization (M), saturation magnetization (M_s), remanent magnetization (M_r) and coercivity (H_c) are summarized in Table 2.

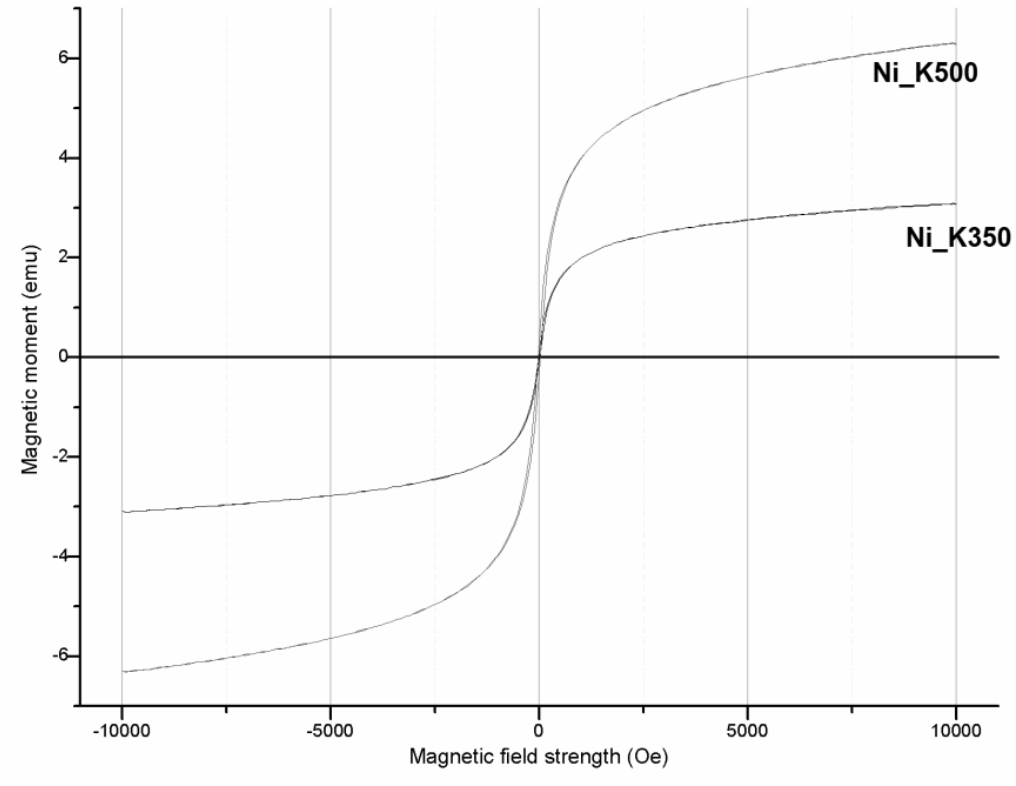

Fig. 7 – Magnetization versus applied magnetic field of obtained composites.

Table 3

Magnetization data of the composites

Sample	Specific magnetization at 10kOe (*M*) emu/g	Saturation magnetization (M_s) emu/g	Remanent magnetization (M_r) emu/g	Coercivity (H_c) Oe
Ni_K350	3.08	3.49	10.57	0.09
Ni_K500	6.30	7.11	21.41	0.32

It can be observed that the investigated compounds produce a very narrow hysteresis cycle, indicating a behavior characteristic to soft magnetic materials. Moreover, the magnetic properties of the compounds proved the ferromagnetic nature of the materials. The shape and width of the hysteresis cycle are a consequence of the several factors, such as synthesis technique, chemical composition, cation distribution, crystallite size.[40] The magnetization of ferrites is dependent on the ion species present and their distribution in the lattices, as well as on the particle size. An increase in the size of the particles leads to higher magnetization.[17,41] The values shown in Table 3 confirm all such statements, *i.e.* the composite containing nickel ferrite, which was calcinated at 500°C, with a bigger particle size, has the best magnetic behavior. The composite showed an increase in saturation magnetization (M_s) and coercive field (H_c) at 10 kOe when calcinated at 500°C. This behavior can be explained by higher crystallinity of nickel ferrite particles.

2. Evaluation of adsorptive activity

The adsorptive activity of the new composites prepared was evaluated at pH= 3 under visible light, through monitoring of the methyl orange (MO) dye decomposition, as a function of the irradiation time. Changes in the UV-Vis spectra at various time intervals (0, 30, 40, 60, 90 and 120 min of contact time between dye and composite) are presented in Fig. 8. The resulting spectra show a rapid decrease in the concentration of MO, meaning that the degradation process (adsorption on catalysts surface) starts immediately after adsorbent immersion. Increasing the contact time between composite and MO leads to an increase in the adsorptive performance of both Ni_K350 and Ni_K500.

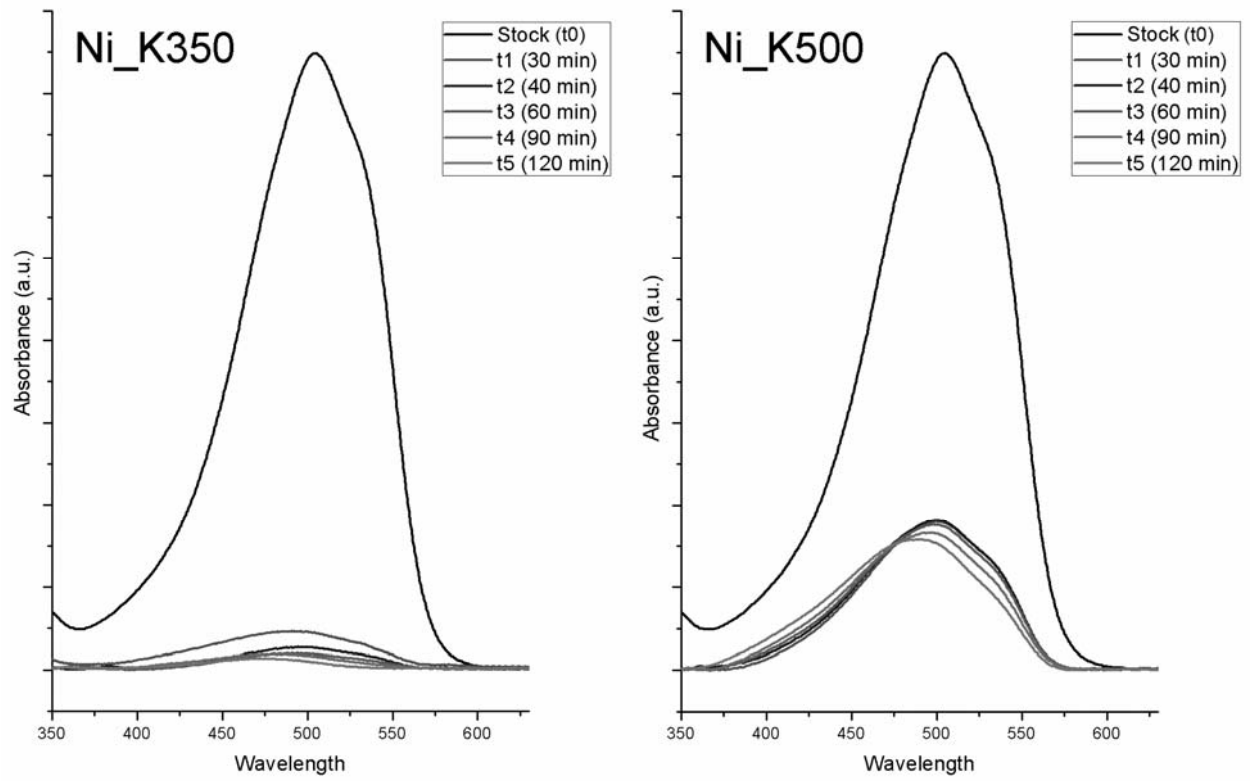

Fig. 8 – UV-vis spectra of MO solution and composites.

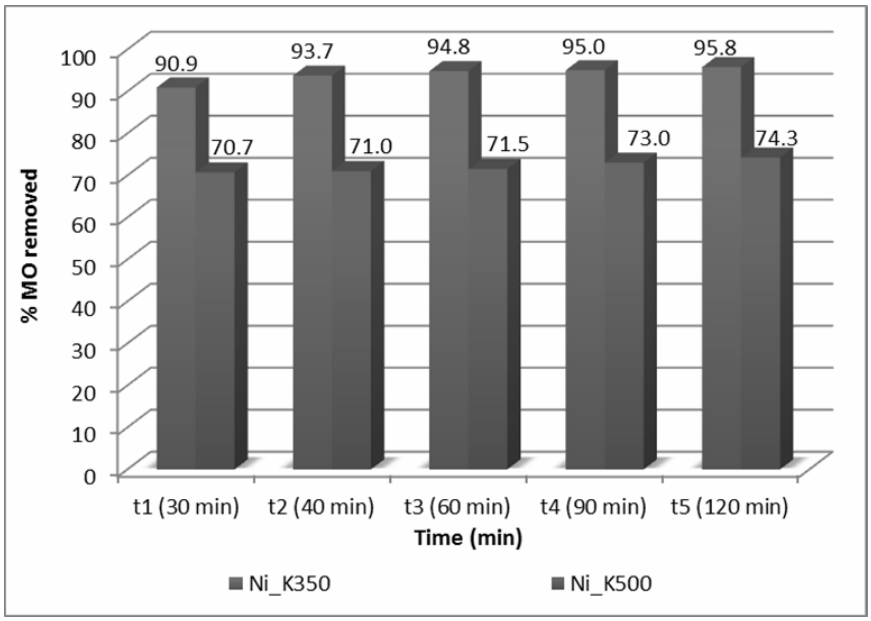

Fig. 9 – Percentage of dye degraded by the composites.

Both adsorption and catalytic degradation of dye molecules on the surface of the composites prepared can be greatly affected by the thermal treatment applied to the sample, as shown in Fig. 9. A large percent of the MO molecules can be adsorbed on the composites especially when the materials are calcinated at low temperatures (e.g. 350°C). In this case, the adsorption efficiency is in accordance to the surface area of the materials and crystallization degree of $NiFe_2O_4$. If adding Ni_K350 sample to the solution led to a dye removal percentage of 95.8 % after 120 minutes, while Ni_K500 removed only 74.3% of dye at the same time interval. The enlarging crystallite size,

particle aggregation and shrinking surface area at high temperature are detrimental to the removal of MO from the solution. The change in MO color is clearly visible to the eye (Fig. 10), but also noticeable in the UV-vis spectra. If the stock methyl orange solution at pH 3 has a slight pink-orange hue, at lower values of MO concentration the solution has a more yellow-orange coloration. This leads to a shift in the spectra wavelength at which the MO peak is identified to lower wavelength, as the solution decolorizes.

In order to assess the decomposition rate of methyl orange, plots of (Ct/C0) and ln(Ct/C0) versus time have been plotted (Fig. 11 and Fig. 12), where C0 and Ct represent the concentrations of the dye before and after adsorption experiments. The degradation kinetics of methyl orange follows the first order kinetic model:

$$\ln Ct/C0 = -kt$$

where k is the apparent reaction constant and t is the chosen reaction time. The adsorption results were noticeably better for the composite material obtained at 350°C, with the largest amount of dye removed in the first 30 minutes of the experiment. It can be observed that, for both samples, the best performance was achieved after 120 minutes of contact time, with first order kinetic rate constant k of 0.491×10^2 for Ni_K350 and 1.44×10^2 for Ni_K500.

The combination of clay and ferrite, and thus the formation of magnetic composites (Ni_K350 and Ni_K500) has probably led to the formation of a large number of charged groups on the clay surface which increases the electrostatic attraction between the positively charged dyes and negatively charged surface of composite. Hence, these $NiFe_2O_4$/clay composites exhibit high adsorption efficiencies.[6]

Fig. 10 – MO initial color (t0, left) and after 120 min (t5, right) after Ni_K350 adsorption.

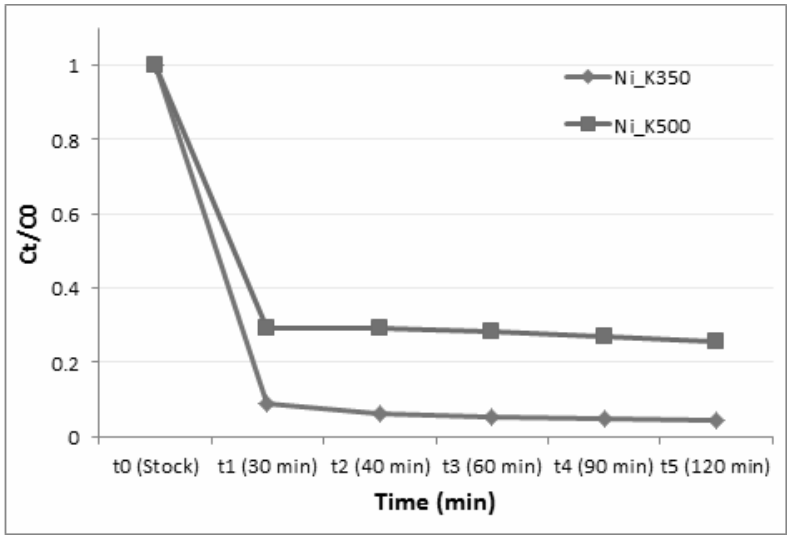

Fig. 11 – Adsorptive degradation of MO dye.

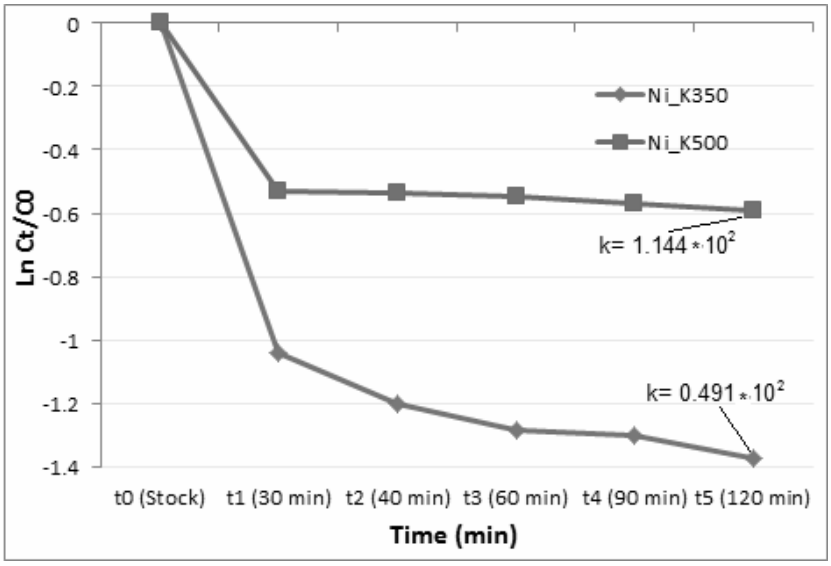

Fig. 12 – Degradation kinetics of MO dye.

CONCLUSIONS

The adsorptive abilities of novel $NiFe_2O_4$/kaolinite composites was examined in the degradation of Methyl orange dye in aqueous solution, under normal conditions of temperature and in the presence of natural visible light. The XRD and FTIR characterization of the composites (Ni_K350 and Ni_K500) revealed the presence of species, clay and ferrite, in the final product. The magnetization measurements showed that the composites exhibited magnetic characteristics relating to soft magnetic materials. SEM, TEM and nitrogen adsorption-desorption isotherms indicated that the composites have promising textural properties, suitable to be applied in the removal of organic dyes from water. The best removal efficiency was obtained for Ni_K350, the sample with the largest BET surface of 67 m²/g. After 120 minutes of contact time, 95.8% of MO was removed from the solution. The dye discoloration tests also revealed that the largest percentage of MO is removed in the first 30 minutes, for both composites. The newly formed materials can be successfully applied in the field of environmental remediation, due to their excellent adsorbent capacity as well as magnetic characteristics, which enable them to be easily recovered after depollution.

Acknowledgements: This work was supported by the strategic grant POSDRU/159/1.5/S/133391, Project "Doctoral and Post-doctoral programs of excellence for highly qualified human resources training for research in the field of Life sciences, Environment and Earth Science" cofinanced by the European Social Fund within the Sectorial Operational Program Human Resources Development 2007 – 2013.

REFERENCES

1. R. Gong, M. Li, C. Yang, Y. Sun and J. Chen, *J. Hazard. Mater.,* **2005**, *121*, 247–250.
2. L. C. a Oliveira, R. V. R. a Rios, J. D. Fabris, K. Sapag, V. K. Garg and R. M. Lago, *Appl. Clay Sci.,* **2003**, *22*, 169–177.
3. M. Nikazar, K. Gholivand and K. Mahanpoor, *Desalination,* **2008**, *219*, 293–300.
4. N. M. Mahmoodi, *J. Taiwan Inst. Chem. Eng.,* **2013**, *44*, 322–330.
5. R. Marandi, A. Abdollah, M. Sharif, M. E. Olya and R. Moradi, *J. Basic. Appl. Sci. Res.*, **2013**, *3*, 443–456.
6. A. Tadjarodi, M. Imani and M. Salehi, *RSC Adv.,* **2015**, *5*, 56145–56156.
7. H. Zhao, Y. Dong, G. Wang, P. Jiang, J. Zhang, L. Wu and K. Li, *Chem. Eng. J.,* **2013**, *219*, 295–302.
8. I. Ullah, S. Ali, M. A. Hanif and S. A. Shahid, *IJCBS,* **2012**, *2*, 60–77.
9. J. Feng, X. Hu, P. L. Yue, H. Y. Zhu and G. Q. Lu, *Chem. Eng. Sci.,* **2003**, *58*, 679–685.
10. I. Fatimah, *J. Adv. Res.,* **2014**, *5*, 663–670.
11. T. Shanmugavel, S. Gokul Raj, G. Ramesh Kumar, G. Rajarajan and D. Saravanan, *J. King Saud Univ. - Sci.,* **2015**, *27*, 176–181.
12. R. Hsu, W. Chang and J. Lin, *Appl. Mater. Interface.,* **2010**, 1349.
13. H. Mao, X. Liu, J. Yang, B. Li, C. Yao and Y. Kong, *Mater. Sci. Eng. C,* **2014**, *40*, 102–108.
14. J. Zarzycki, *J. Sol-Gel Sci. Technol.,* **1997**, *8*, 17–22.
15. Ş. Cojocaru, A. M. Dumitrescu, I. G. Breabăn, A.-A. Domocos, N. Melniciuc-Puică, A. R. Iordan and M. N. Palamaru, *Optoelectron. Adv. Mater. - Rapid Commun.,* **2015**, *9*, 1530–1534.
16. A. E. Lavat and E. J. Baran, *J. Alloys Compd.,* **2006**, *419*, 334–336.
17. T. Slatineanu, A. R. Iordan, M. N. Palamaru, O. F. Caltun, V. Gafton and L. Leontie, *Mater. Res. Bull.,* **2011**, *46*, 1455–1460.
18. A. Pradeep, P. Priyadharsini and G. Chandrasekaran, *J. Magn. Magn. Mater.,* **2008**, *320*, 2774–2779.

19. F. Wypych and K. G. Satyanarayana, *J. Colloid Interface Sci.,* **2005**, *285*, 532–543.
20. H. W. van der Marel and H. Beutelspacher, "Atlas of Infrared Spectroscopy of Clay Minerals and their Admixtures", Amsterdam, Elsevier Sci. Ltd., 1976.
21. K. Mamulová Kutláková, J. Tokarský and P. Peikertová, *Appl. Catal. B Environ.,* **2015**, *162*, 392–400.
22. Y. H. Kim, M. S. Hwang, H. J. Kim, J. Y. Kim and Y. Lee, *J. Appl. Phys.,* **2001**, *90*, 3367–3370.
23. V. C. Farmer, *Clay Miner.,* **1968**, *7*, 373–387.
24. R. Prost, A. Dameme, E. Huard, J. Driard and J. P. Leydecker, *Clays Clay Miner.,* **1989**, *37*, 464–468.
25. A. Tironi, M. A. Trezza, E. F. Irassar and A. N. Scian, *Procedia Mater. Sci.,* **2012**, *1*, 343–350.
26. A. K. Panda, B. G. Mishra, D. K. Mishra and R. K. Singh, *Colloids Surfaces A Physicochem. Eng. Asp.,* **2010**, *363*, 98–104.
27. R. Duarte-Silva, M. A. Villa-García, M. Rendueles and M. Díaz, *Appl. Clay Sci.,* **2014**, *90*, 73–80.
28. E. Escalera, R. Tegman, M. L. Antti and M. Odén, *Appl. Clay Sci.,* **2014**, DOI 10.1016/j.clay.2014.07.024.
29. A. Shvarzman, K. Kovler, G. S. Grader and G. E. Shter, *Cem. Concr. Res.,* **2003**, *33*, 405–416.
30. R. Fernandez, F. Martirena and K. L. Scrivener, *Cem. Concr. Res.,* **2011**, *41*, 113–122.
31. R. Frost and A. M. Vassallo, *Clays Clay Miner.,* **1996**, *44*, 635–651.
32. D. Yeskis, A. F. K. Van Groos and S. Guggenheim, *Am. Mineral.,* **1985**, *70*, 159–164.
33. M. C. Gastuche, F. Toussaint and J. J. Fripiat, *Clay Miner.,* **1963**, 227–236.
34. B. R. Ilić, A. A. Mitrović and L. R. Miličić, *Hem. Ind.,* **2010**, *64*, 351–356.
35. R. Luque, J. M. Campelo, D. Luna, J. M. Marinas and A. A. Romero, *J. Mol. Catal. A Chem.,* **2007**, *269*, 190–196.
36. W. Walerczyk, M. Zawadzki and H. Grabowska, *Catal. Letters,* **2012**, *142*, 71–80.
37. R. Cisneros, H. Pfeiffer and C. Wang, *Nanoscale Res. Lett.,* **2010**, *5*, 686–691.
38. J. Feng, X. Hu and P. L. Yue, *Environ. Sci. Technol.,* **2004**, *38*, 269–275.
39. A. I. Borhan, P. Samoila, V. Hulea, A. R. Iordan and M. N. Palamaru, *J. Photochem. Photobiol. A Chem.,* **2014**, *279*, 17–23.
40. A. I. Borhan, T. Slatineanu, A. R. Iordan and M. N. Palamaru, *Polyhedron,* **2013**, *56*, 82–89.
41. F. Grasset, N. Labhsetwar, D. Li, D. C. Park, N. Saito, H. Haneda, O. Cador, T. Roisnel, S. Mornet, E. Duguet, J. Portier and J. Etourneau, *Langmuir,* **2002**, *18*, 8209–8216.